2008 20th International Lightning Detection Conference
21-23 April • Tucson, Arizona, USA
2nd International Lightning Meteorology Conference
24-25 April • Tucson, Arizona, USA

UPDATE TO THE LIGHTNING PROBABILITY FORECAST EQUATIONS AT KENNEDY SPACE CENTER/CAPE CANAVERAL AIR FORCE STATION, FLORIDA

Winifred Lambert
NASA Applied Meteorology Unit / ENSCO, Inc. / Cape Canaveral Air Force Station, Florida

William Roeder
USAF 45th Weather Squadron / Patrick Air Force Base, Florida

1. INTRODUCTION

The 45th Weather Squadron (45 WS) provides weather support to Kennedy Space Center (KSC) and Cape Canaveral Air Force Station (CCAFS) (Harms et al. 1999). Part of those weather services include a probability of lightning occurrence in the daily 24-Hour and Weekly Planning forecasts, which are briefed in the morning at 1100 UTC (0700 EDT). The probability of lightning occurrence is used in planning for daily ground operation activities on KSC and CCAFS, as the first step leading to local lightning watches and warnings (Weems et al. 2001), and as part of forecasting the lightning launch commit criteria (Roeder and McNamara 2006).

Until completion of the Phase II work described herein, the lightning probability forecast was based on a subjective analysis of model and observational data and the output from an objective lightning forecast tool developed by the Applied Meteorology Unit (AMU) (Bauman et al. 2004) in Phase I (Lambert and Wheeler 2005). This tool was a set of five equations, one for each of the warm season months May–September, that provided a probability of lightning occurrence for the day on KSC/CCAFS. The forecasters accessed the equations through a Microsoft® Excel© graphical user interface (GUI) by entering predictor values. These equations exhibited a large improvement in performance over other standard forecast methods in use and were transitioned to operations in time for the 2005 warm season.

Since the Phase I equations were developed, new ideas regarding certain predictors were formulated and a desire to make the tool more automated was expressed by 45 WS forecasters. They anticipated that modifying the predictors would improve tool performance, and automating the tool would reduce the time spent producing the forecasts and decrease the likelihood of human error in entering values. Phase II, therefore, had two parts: 1) to re-examine and modify the calculation method of certain predictors and to use the modified predictors in developing new monthly equations, and 2) to create an automated tool in the current operational weather display system for the 45 WS, the Meteorological Interactive Data Display System (MIDDS).

2. DATA

The Period of Record (POR) for the data increased from 15 to 17 years and included warm season data in the years 1989 – 2005. The data sources were the

- Cloud-to-Ground Lightning Surveillance System (CGLSS),
- 1200 UTC Jacksonville (JAX), Tampa (TBW), and Miami (MFL) soundings, and
- 1000 UTC CCAFS (XMR) sounding.

2.1 Cloud-to-Ground Lightning Surveillance System (CGLSS)

The CGLSS is a network of six sensors (Figure 1) that collects date, time, latitude, longitude, strength, and polarity information of cloud-to-ground (CG) lightning strikes in the local KSC/CCAFS area (Boyd et al. 2005). The CGLSS data were used to determine whether or not lightning occurred on each day in the POR. The purpose of the CGLSS data was to create the binary predictand for the equations. The data were also used to create a daily climatological frequency and persistence forecasts that would be used as candidate predictors and forecast benchmarks against which to test the new equations.

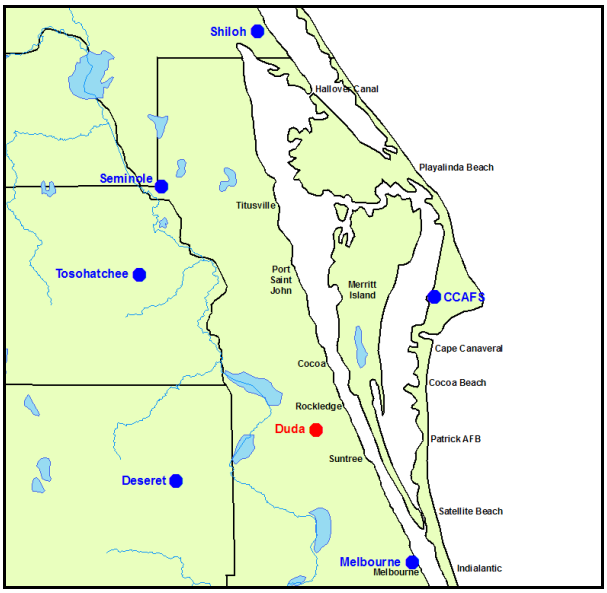

Figure 1. The CGLSS network sensors are indicated by the blue dots. The location names are next to the circles. The Duda sensor (red circle) was moved to the Deseret site in 2005.

2.2 Florida 1200 UTC Rawinsondes

These data were collected to determine the daily flow regimes using the procedure outlined in Lericos et al. (2002), which based the flow regime on the mean wind direction in the 1000–700 mb layer. As noted in Lericos, the current MFL and JAX sites were located at West Palm Beach, FL (PBI) and Waycross, GA (AYS), respectively, prior to 1995. The PBI and AYS data were used as proxies for MFL and JAX, respectively, during the period 1989–1994. The map in Figure 2 shows the locations of all the soundings used in this task.

Use of the 1200 UTC sounding may seem inappropriate as it cannot provide data in time for the 1100 UTC briefing. Use of the 0000 UTC sounding from the day before was ruled out as the 1000–700 mb flow during the Florida warm season could be contaminated by afternoon convective circulations that mask the larger scale flow pattern. For the purpose of determining the flow regimes for each day in the POR, the 1200 UTC sounding provided the most reliable data. Due to the weak synoptic patterns during the Florida warm season, it is not likely that a flow regime change would take place in the two-hour period between 1000–1200 UTC. In an operational setting, the 45 WS can use several data sources, including model output and surface observations, to help determine the flow regime of the day before the morning 1100 UTC briefing.

2.3 XMR 1000 UTC Sounding

The 45 WS forecasters use data from the XMR 1000 UTC sounding for the 1100 UTC morning briefing since it contains the most recent information on the state of the atmosphere over the area. These data were used to calculate the sounding parameters normally available to the forecasters through MIDDS. The parameters were used as candidate predictors in the equation development. The XMR soundings were also used to determine the flow regime of the day with the 1200 UTC JAX, TBW, and MFL soundings. The procedure is discussed in Section 3.3.

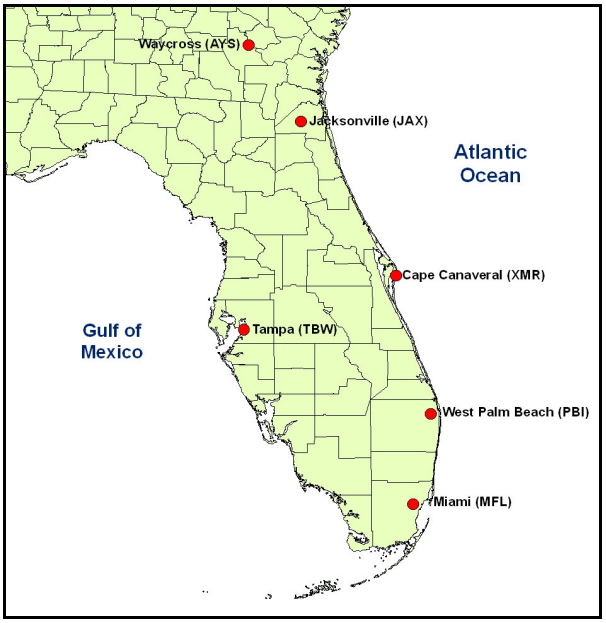

Figure 2. The red dots on the map show the locations of all soundings used in this work.

3. MODIFICATIONS

As stated in Section 1, the 45 WS requested modifications to the Phase I data and candidate predictors that could improve their performance. Specifically, they requested five modifications:

- Increase the POR by two years,
- Modify the valid area,
- Use the XMR 1000 UTC sounding to help determine the flow regime of the day,
- Use different smoothing values for the daily climatology, and
- Determine an optimal layer for the average RH calculation.

3.1 Increased POR

Two more warm seasons occurred since the Phase I equations were developed. The new POR now includes data from all the warm seasons in the years 1989–2005. This increased the POR from 15 to 17 years and was expected to produce more robust statistics in the development of the equations.

3.2 New Valid Area

The equations are meant to forecast lightning occurrence within 5 n mi-radius warning circles surrounding specific asset locations (Figure 3). The valid area for CG lightning occurrence in Phase I was the entire area shown in Figure 3, a rectangle surrounding all 5 n mi warning circles including Astrotech. For Phase II, the 45 WS requested that the valid area be reduced to include only the 10 circles on KSC (blue circles) and CCAFS (red circles) to the right of the vertical black line in Figure 3. While the 45 WS has a warning responsibility for Astrotech, that area is not included in their daily planning forecasts.

The AMU used an algorithm that calculated the distance of each CG strike from the center of each of the 10 circles. The latitude/longitude (lat/lon) values from the CGLSS data and the center lat/lon of all 10 circles were used in the Great Circle Distance Formula:

$$D = 3437.75 * \arccos[\sin(lat1) * \sin(lat2) + \cos(lat1) * \cos(lat2) * \cos(lon2-lon1)]$$

(http://www.meridianworlddata.com/distance-calculation.asp),

where D is the distance between the strike and the circle in n mi, lat1/lon1 is the lat/lon of the circle center, lat2/lon2 is the lat/lon of the strike, and all lat/lon values are in radians. A day on which CG lightning were within any circle (D ≤ 5 n mi) was considered a lightning day. The number of strikes was not considered for the lightning probabilities.

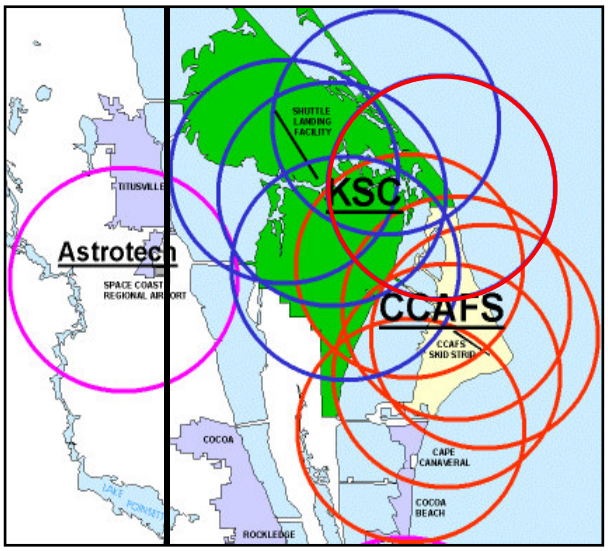

Figure 3. The 5 n mi lightning warning circles surrounding KSC/CCAFS and Astrotech. The valid area for the Phase II work is within the four blue (KSC) and six red (CCAFS) circles with centers to the right of the vertical black line.

3.3 Flow Regime Discriminator

Table 1 shows the definitions for the flow regimes used in both Phases. After stratifying the days by flow regime in Phase 1, the AMU found that 44% of the days could not be categorized into any of the defined regimes. Given that lightning occurred on 45% of those days, they could not be neglected. Therefore, the AMU stratified them into a new flow regime category named 'Other'. The 45 WS suggested using the 1000–700 mb mean wind direction in the 1000 UTC XMR sounding to determine a flow regime for the 'Other' days in the Phase II work to reduce the number of days in 'Other' and increase the number of days in the defined categories so that more robust statistics could be calculated.

Table 1. List of the flow regime names used in Phases I and II and the corresponding sectors showing the average 1000–700 mb wind directions at each of the stations.

Flow Regime Name and Description		***Rawinsonde Station***		
		MFL	**TBW**	**JAX**
SW-1	Subtropical ridge south of MFL Southwest flow over KSC/CCAFS	180°-270°	180°-270°	180°-270°
SW-2	Subtropical ridge north of MFL, south of TBW Southwest flow over KSC/CCAFS	90°-180°	180°-270°	180°-270°
SE-1	Subtropical ridge north of TBW, south of JAX Southeast flow over KSC/CCAFS	90°-180°	90°-180°	180°-270°
SE-2	Subtropical ridge north of JAX Southeast flow over KSC/CCAFS	90°-180°	90°-180°	90°-180°
NW	Northwest flow over Florida	270°-360°	270°-360°	270°-360°
NE	Northeast flow over Florida	0°-90°	0°-90°	0°-90°
Other	When the layer-averaged wind directions at the three stations did not fit in defined flow regime			
Missing	One or more soundings missing			

The synoptic flow regime was determined first by using a combination of the average 1000–700 mb wind directions from the 1200 UTC MFL, TBW, and JAX soundings, as outlined in Lericos et al. (2002). The wind speeds and directions were decomposed into u- and v-components, and then the layer-average u-and v-winds were calculated and recombined to get an average wind speed and direction at each individual location. Then, the average 1000–700 mb wind direction in the 1000 UTC XMR sounding was calculated and used to determine the 'local' flow regime of the day. This was the discriminator in determining the final flow regime of the day. This procedure reduced the number of 'Other' cases by ~70% and distributed those cases among the SW, SE, NW, and NE regimes.

3.4 Smoother for Daily Climatology

The daily climatology values were important predictors in all five Phase I equations, and were also used as forecast benchmarks when testing the performance of the equations.

The number of years that each day experienced lightning was determined, and a raw climatology was calculated by dividing this number by 17, the number of years in the POR. This yielded a fractional value between 0 and 1 for each day. The thin blue jagged curve in Figure 4a is the raw 17-year climatology for each day in the warm season. The noisy appearance of this curve is likely due to the few number of years in the POR; 17 is a small number of observations from which to calculate a climatology. A common procedure to minimize the noisiness of such a curve is to use a weighted average of the observations several days before and after the day of interest, artificially increasing the number of observations used in order to smooth out the curve and infer what the long-term climatology would be if enough observations were available. A Gaussian weighting function was used to smooth the curve, defined by the equation

$$P = \frac{1}{N}\left\{\frac{\sum_{k=0}^{m}\left[W(F_{n-k}+F_{n+k})\right]+F_n}{\sum_{k=0}^{m}\left[W*2\right]+1}\right\}$$ (Everitt 1999),

where W is the Gaussian weighting function

$$W = \exp\left[\frac{-\left(k^2\right)}{2*\sigma^2}\right]$$ (Wilks 2006),

P = climatological probability on the day of interest,
N = number of years in the POR (17),
n = day number of interest,
k = number of days distant from n,
m = maximum ± number of days distant from n,
F = raw probability on day of interest, and
σ = scale factor in units of days.

Using the Phase I values m = ±7 and σ = 3 days for the 17-year POR resulted in the smoother red curve in Figure 4a that was still somewhat noisy. The 45 WS tested several combinations and suggested m = ±14 and σ = 7 days to provide the best combination of smoothness with minimal changing of the raw data. This created a smooth curve, represented by the thick blue curve in Figure 4a. The values for W are in Figure 4b.

3.5 Optimal Relative Humidity Layer

The average RH in the 800–600 mb layer was an important predictor in four of the five Phase I equations. This parameter was determined as valuable in the study that created the Neumann-Pfeffer Thunderstorm Index (NPTI) (Neumann 1971) over 30 years ago. It has been used in several studies since that time, but no rigorous attempts have been made to determine if 800–600 mb is the optimal layer for this parameter.

An iterative technique was used to determine the optimal layer using the 1000 UTC XMR sounding. It began by calculating the average RH in all 200-mb layers between 950 mb as the lowest base and 400 mb as the highest top, incrementing the base and top of each layer by 25 mb. This resulted in 15 layers. The average RH in each of the layers was calculated with a log(p)-weighted averaging method using all levels in the layer. The region of influence, D_i, for each RH observation in the sounding was defined as

$$D_i = \frac{[\log(p_{i-1}) - \log(p_{i+1})]}{2},$$

where 'i' is the level number, p_{i-1} is the pressure at the observation directly below and p_{i+1} is the pressure directly above p_i. The average RH for each 200-mb layer was calculated with the equation

$$RH_{avg} = \frac{\sum(RH_i * D_i)}{\sum D_i}.$$

The 200-mb layer average RH with the highest correlation to lightning occurrence was 775–575 mb, with a center at 675 mb.

The iterative technique began anew, centered at 675 mb and adding layers in 25 mb increments above and below to find an optimal thickness. This procedure yielded the 825–525 mb layer average RH as the most highly correlated to lightning occurrence. This is close to the original 200-mb thick layer of 800–600 mb. The new layer is 300-mb thick.

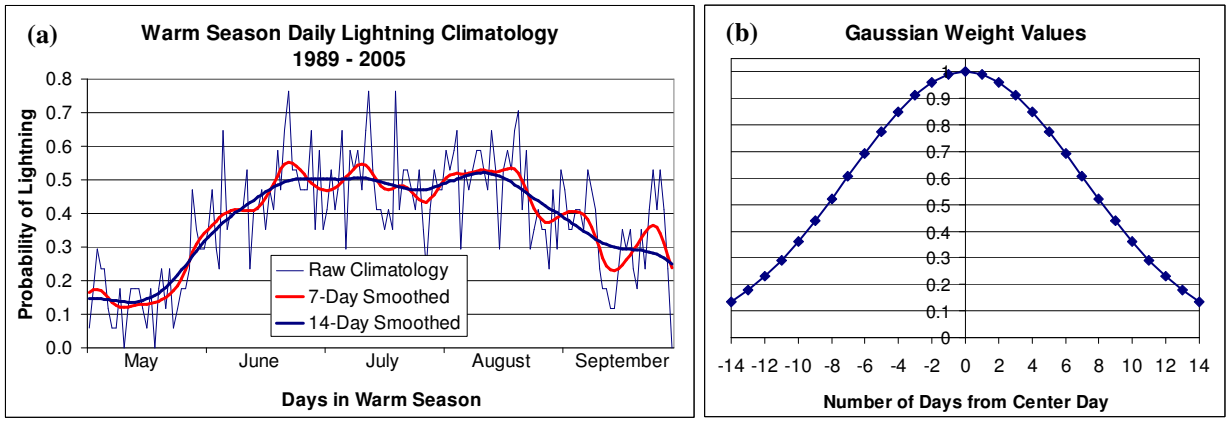

Figure 4. (a) The daily raw (thin blue curve), ±7-day smoothed (red curve), and ±14-day smoothed (thick blue curve) climatological probability values of lightning occurrence for the warm-season months in 1989–2005, and (b) The Gaussian weight values (W) used in the ±14-day smoothing equation.

4. EQUATION ELEMENTS

The datasets described in Section 2 were processed with the modifications described in Section 3 to create the elements needed for the statistical forecast equation development. The necessary elements include a predictand and candidate predictors. The predictand is the element to be predicted from a predictor or group of predictors.

4.1 Binary Predictand

The CGLSS data were filtered spatially to include only strikes that occurred within the 10 5-n mi warning circles shown in Figure 3. Then they were filtered temporally to include only lightning strikes recorded in the time period 0700–0000 EDT. The 45 WS morning forecast is issued at 0700 EDT and is valid for 24 hours. However, the 45 WS verification procedure is for the current day, or Day 1, to end at midnight (0000 EDT). They consider times after midnight as Day 2. Since the goal of this task was to develop equations for Day 1 forecasts, lightning occurring between midnight and 0700 EDT were not considered.

Once the data were filtered, the value of the binary predictand was set to '1' if lightning was detected within the defined time period and area on each day, otherwise a '0' was assigned. A binary predictand was used because the prediction is for lightning occurrence, not the number of strikes. The 45 WS verification procedure only requires one strike for a lightning warning to be validated.

4.2 Candidate Predictors

The list of candidate predictors included 1-day persistence and daily climatological lightning frequency (Figure 4) determined from the CGLSS binary predictand, the flow regime probabilities from the soundings and CGLSS binary predictand, and 11 stability parameters calculated from the XMR sounding.

CGLSS Predictors

The binary predictand discussed in Section 4.1 was used to create two candidate predictors: a binary 1-day persistence and the daily climatological probability of lightning occurrence described in Section 3.4. Calculation of the persistence predictor was straightforward. If lightning occurred on a particular day, the persistence value for the next day was '1'. If lightning did not occur, the persistence value was '0'. The lightning occurrence information for April 30 was used to create the persistence value for May 1. The values along the thick blue curve in Figure 4a were used for the daily climatological values of lightning probability.

Flow Regime Probabilities

The AMU determined a flow regime for each day using the morning JAX, TBW, MFL, and XMR soundings as described in Section 3.3. Then, the probabilities of lightning occurrence based on flow regime for each month and the entire warm season were calculated using the CGLSS binary predictand. The number of days that each regime occurred was compared to the CGLSS predictand to see how many of those days experienced lightning. The climatological probability was calculated by dividing the number of lightning days within a particular regime by the total number of days the regime occurred.

The lightning probability values are shown in Table 2. The values for each flow regime in each month (columns 2–7) were used as candidate predictors in the equation development. The overall monthly climatologies (column 8) were used as forecast benchmarks in determining the skill of the equations.

The SW-1 and SW-2 values for each month were within 10% of each other. Therefore, the SW-1 and SW-2 days in each month were combined to increase the sample size and produce a more reliable probability value. The resulting combined SW-1/2 values for June, July, and August were also within 10% of each other, therefore the days for these flow regimes and months were combined to create one SW value for those three months. In June–August, the SE-1 and SE-2 regimes were also within 10%, so their values were combined to create one SE flow regime value for all three months. This was not the case for the May and September SE regimes. The parentheses around the SE-2 values for June–August indicate that it is a combined value and the same as SE-1.

Table 2. Monthly probabilities of lightning occurrence based on the flow regimes that were used as candidate predictors. The values in the far-right column are the monthly probabilities for all flow regimes combined, and were used as a forecast benchmark.

Month	SW-1/2	SE-1	SE-2	NW	NE	Other	Monthly
May	30	19	6	16	2	16	18
June	68	32	(32)	46	11	30	46
July	68	32	(32)	53	14	43	48
August	68	32	(32)	38	12	55	49
September	55	42	29	16	17	24	33

Stability Indices

The stability indices calculated from the 1000 UTC XMR sounding were those normally available to the forecasters through MIDDS. In order to calculate the same values that would be available to the forecasters, the same equations used in the MIDDS code were used. The stability index candidate predictors included

- Total Totals (TT),
- Cross Totals (CT),
- Vertical Totals (VT),
- K-Index (KI),
- Lifted Index (LI),
- Thompson Index (TI),
- Severe Weather ThrEAT Index (SWEAT),
- Showalter Stability Index (SSI),
- Temperature at 500 mb (T_{500}),
- Mean Relative Humidity in the 825–525 mb layer (MRH), and
- Precipitable water up to 500 mb (PW),

Previous studies and local experience have shown the KI and LI to be useful in predicting the likelihood of thunderstorms at KSC/CCAFS (Kelly et al. 1998, Howell 1998, and Everitt 1999). The TI should also be a good predictor since it is the difference between KI and LI. The other stability indexes were included as candidate predictors to provide an unbiased and complete selection.

The MIDDS uses the Man-computer Interactive Data Access System (McIDAS) software (Lazzara et al. 1999) for processing sounding data. The formulas in the McIDAS code used for the indices are standard and can be found in several sources (e.g. Peppler and Lamb 1989; Ohio State University Severe Weather Products web page at http://twister.sbs.ohio-state.edu).

5. EQUATION DEVELOPMENT AND TESTING

The AMU developed a set of five equations, one for each month in the warm season. The performance of the equations was assessed using several verification techniques appropriate for probability forecasts.

5.1 Development and Verification Datasets

Of the 17 warm seasons in the POR, 14 were used for equation development and 3 were set aside for equation verification. This ensured that each month in the warm season was equally represented in both datasets.

The stratification did not involve choosing individual warm season years for each dataset, but rather individual warm season days were chosen randomly. Days for the verification dataset were chosen first. Given that there are 153 days in the warm season, the random number generator in Excel was used to create three sets of 153 numbers representing the years 1989 – 2005. The resulting three sets of years were assigned to each day in the warm season. Thus, each day in the warm season was represented by days from three random years. Care was taken to ensure the there were no duplicate years for each day from the random number generator. As an example, the verification dataset contains 1 May 1989/1999/2001,

2 May 1993/1998/2000, etc. All other dates were made part of the development dataset. This random-day method was chosen to reduce the likelihood that any unusual convective seasons would bias the results.

5.2 Equation Development

Final predictor selection was conducted for each individual month due to the possibility that different variables may become more critical to convection formation as the warm season progresses.

Logistic Regression

According to Wilks (2006), logistic regression is the appropriate method when the predictand is binary. Logistic regression was chosen as the statistical method in Phase I due to the binary nature of the predictand and also due to results from a previous study. Everitt (1999) showed that logistic regression yielded 48% better skill over the linear regression equations in NPTI when using the same predictor variables and data. The gain in skill was due solely to use of the logistic regression method. Given a predictand, y, and a set of predictors $x_{1...}x_k$, where k is the total number of predictors, logistic regression is represented by

$$y = \frac{e^{(b_0+b_1x_1+...+b_kx_k)}}{1+e^{(b_0+b_1x_1+...+b_kx_k)}},$$

where $b_1 \ldots b_k$ are the coefficients for the corresponding predictors.

Residual Deviance Calculation

The contribution of each candidate predictor to the reduction in variance was determined by the residual deviance. The parameter serves the same role in logistic regression as does the residual sum of squares in a linear regression (Insightful Corporation 2005a). Menard (2000) examined several methods that help determine the amount of predictand variance explained by predictors in logistic regression equations. The preferred method in that study was determining the percentage drop in the residual deviance when a new predictor was added. Therefore, it was the method employed in Phases I and II.

Predictor Selection

The procedure to develop a logistic regression equation outlined in the S-PLUS User's Manual (Insightful Corporation 2005b) was used to create the equations. The candidate predictors were added to a logistic regression equation one-by-one and their contribution to the reduction in residual deviance noted. While more automatic predictor selection methods in S-PLUS could have been employed, this manual process allowed for more control over understanding how each candidate predictor contributed to the reduction in residual deviance individually and in combination with other predictors. It was also facilitated by the relatively small number of candidate predictors available for selection.

The single candidate predictor that affected the largest reduction in the residual deviance was chosen as the first predictor in the equation. The second candidate predictor that reduced the residual deviance by the largest amount in combination with the first was chosen as the second predictor. This process was followed using all candidate predictors. Figure 5 shows the percent reduction in residual deviance from the NULL model from the first eight predictors added for June as an example. The TI reduced the residual deviance by the most (19%) and was, therefore, the first predictor. The second predictor was the flow regime lightning probability (FRProb in Figure 5), which accounted for an additional 9% reduction in residual deviance. The third predictor was persistence (Pers in Figure 5), reducing the residual deviance by 1%, and so on.

While all candidate predictors were used in each equation to determine their rank order, all could not be used in the final equations as that could lead to overfitting (Wilks 2006). When this happens, the equations perform well with data from the development dataset, but perform poorly on the verification set. Wilks (2006) suggests several 'stopping rules', the point at which no more predictors will be added to the equation. In Phase II, the AMU used a similar stopping rule to that in Phase I. Scree diagrams showing the reduction in residual deviance, like Figure 5, were created for each month (not shown). The AMU then examined the change in slope of the curves as each predictor was added. The change in the slope of the curve after MRH in Figure 5 is at the point where the residual deviance is reduced by less than 0.5%. Similar changes in slope were found in the other four months for the same cutoff value. The stopping rule was to stop adding predictors when a candidate predictor effected a < 0.5% change in the residual deviance that came

after it. The AMU tested equations with one more and one less predictor than the stopping rule indicated, only to conclude that the equation created with the < 0.5% stopping rule had superior performance.

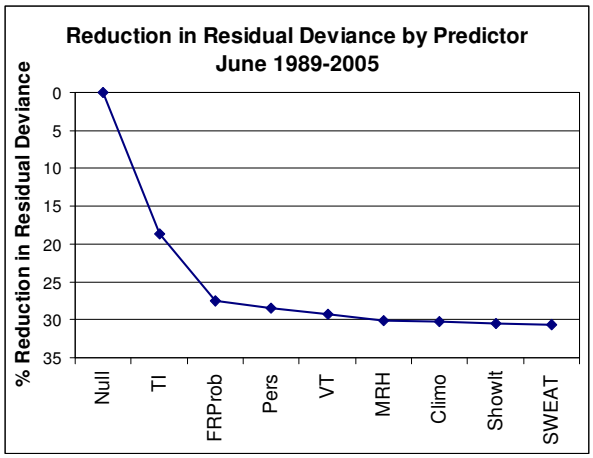

Figure 5. The total percent reduction in residual deviance from that of the NULL model as each predictor was added to the equation using the June development dataset.

Final Predictors

This predictor selection process was repeated for all five months in the warm season. Table 3 shows the final predictors for each of the monthly equations in rank order of their reduction in residual deviance. The predictor names are color-coded according to the number of equations in which they appear. Red indicates that a predictor was chosen in every equation, i.e. it proved useful throughout the entire warm season. There was only one: the probability of lightning occurrence based on the flow regime. It was also ranked second in every month, underscoring its importance as a predictor in the KSC/CCAFS area. Blue identifies the two predictors, VT and persistence, that were chosen in four of the five equations. The July equation did not use VT and the August equation did not use Pers. The July equation did include VT indirectly, given that it is in the equation that calculates TT. The predictors in green were chosen for three of the equations, and they are the daily climatology, TI, and MRH. These are followed by the predictors in black, which were only used in one equation each: KI and TT. The June, July, and August equations did include KI indirectly in the equation for TI.

The most important predictors in the May through August equations, KI or TI, account for instability and moisture in the profile, which are both necessary ingredients for thunderstorm formation. September has MRH as the most important predictor, which only accounts for the mid-level moisture. The fourth predictor, VT, accounts for mid-level instability, but it has a much smaller influence on the probability in September due to its rank. The flow regime probability as the second predictor accounts for the lifting mechanism, or lack thereof, as the low-level flow interacts with the sea breeze that occurs almost daily in the warm season.

Table 3. The final predictors for each monthly equation, in rank order of their reduction in residual deviance. The predictors in red were in every equation, the predictors in blue were in four of the five equations, the predictors in green were in three of the five equations, and the predictors in black were in only one equation.

May	*June*	*July*	*August*	*September*
K-Index	Thompson Index	Thompson Index	Thompson Index	825–525 mb MRH
Flow Regime	Flow Regime	Flow Regime	Flow Regime	Flow Regime
Vertical Totals	Persistence	Total Totals	Daily Climatology	Persistence
Daily Climatology	Vertical Totals	Persistence	825–525 mb MRH	Vertical Totals
Persistence	825–525 mb MRH		Vertical Totals	Daily Climatology

5.3 Equation Performance

The predictors from the verification dataset were used in the equations to produce 'forecast' probabilities. The forecast probabilities were compared with the binary lightning observations in the verification dataset using four tests that measured different aspects of forecast performance. They were the

- Brier Skill Score, which is a measure of equation performance versus other standard forecast methods,
- Distributions of the probability forecasts for days with and without lightning,
- Reliability of the observed lightning frequency as a function of the forecast probability, and
- Categorical contingency table statistics.

Brier Skill Score

This test determined if the P-2 equations showed improvement in skill over five forecast benchmarks:

- Persistence,
- Daily climatology (Figure 4a),
- Flow regime probabilities (Table 2),
- Monthly climatology (Table 2), and
- P-1 equations.

The mean square error (MSE) between the probability forecasts and observations was calculated using the equation

$$\mathrm{MSE} = \frac{1}{n}\sum_{i=1}^{n}(p_i - o_i)^2 \quad \text{(Wilks 2006)},$$

where n is the number of forecast/observation pairs, p_i is the probability associated with the forecast method, and o_i is the corresponding binary lightning observation. The skill of the P-2 equations relative to the five forecast benchmarks was calculated using the equation for the Brier Skill Score (SS):

$$\mathrm{SS} = \left(\frac{\mathrm{MSE}_{eqn} - \mathrm{MSE}_{ref}}{\mathrm{MSE}_{perfect} - \mathrm{MSE}_{ref}}\right) * 100 \quad \text{(Wilks 2006)},(10)$$

where MSE_{eqn} was the MSE of the P-2 equations, MSE_{ref} was the forecast benchmark against which the new equations were tested, and $MSE_{perfect}$ was the MSE of a perfect forecast, which is always 0. The SS represents a percent improvement or degradation in skill of the equation over the reference forecast when it is positive or negative, respectively.

The SS values for each of the monthly P-2 equations and a composite result for the full warm season are shown in Table 4. The P-2 equations show a double-digit improvement in skill for the first four benchmarks in the table, similar to the results for the P-1 equations (Lambert and Wheeler 2005). The P-2 equations also show an 8% improvement in skill over the P-1 equations for the composite warm season. For the individual months, the P-2 equations show an improvement in skill over the P-1 equations for June, July, and September. The values of 0.2% for May and -0.8% for August are very small and indicate similar skill between the two equation sets.

Table 4. The SS values showing the percent improvement (degradation) in skill of the P-2 equations over of persistence, daily and monthly climatologies, flow regime probabilities, and the P-1 equations developed in Lambert and Wheeler (2005). These scores were calculated using the verification data for each month and for the entire warm season (All).

Forecast Method	***May***	***Jun***	***Jul***	***Aug***	***Sep***	***All***
Persistence	28	41	37	47	41	40
Daily Climatology	23	25	24	24	26	25
Monthly Climatology	29	27	34	30	25	29
Flow Regime	16	12	11	18	18	15
P-1 Equations	0.2	5	19	(-0.8)	12	8

Probability Distributions

The P-1 and P-2 equation probability forecasts from the verification dataset were stratified by lightning and non-lightning days, and created a probability distribution for each. Such distributions show how well the equations distinguish between lightning and non-lightning days. Figure 6 shows the probability distributions for lightning days represented by the two red curves, and for non-lightning days represented by the two blue curves. For good performance, one would expect the blue curves to have a maximum in the lower probability values decreasing to a minimum at higher values, and the red curves to have a minimum in the lower probability values increasing to a maximum at the higher values.

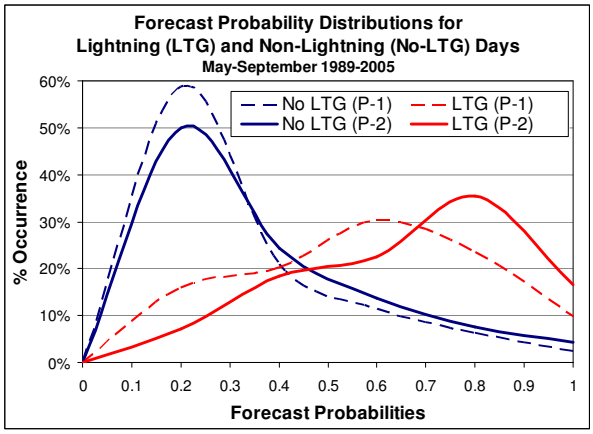

Figure 6. Forecast probability distributions for lightning (red) and non-lightning (blue) days in the verification data. The solid lines represent the P-2 equations and the dashed lines represent the P-1 equations. The y-axis values are the frequency of occurrence of each probability value, and the x-axis values are the forecast probability values output by the equations.

Both blue curves for the non-lightning days in Figure 6 peak at 0.2 probability, decrease rapidly through 0.4, and then decrease more slowly toward 1. This indicates good performance for both equation sets. However, the P-1 equations distinguished non-lightning days with a bit more accuracy as evidenced by the higher peak of 59% versus 50% at 0.2, and the larger drop off to 21% versus 24% to 0.4. The percent occurrence for the P-1 equations remained ~1% below those of the new equations from 0.4 to 1.

The red curve for the P-2 equations indicates that they distinguished lightning days more accurately than the P-1 equations. The percent occurrences of the P-2 probabilities were lower than those for the P-1 equations for all probability values less than 0.7, and higher for all probabilities greater than 0.7. The peak percent occurrence for the P-2 equations was 36% at 0.8 probability, while the peak for the P-1 equations was 30% at 0.6 probability.

Reliability Diagram

A reliability diagram (Wilks 2006) indicates how the equations perform in terms of under- or over-forecasting lightning occurrence at discrete probability values from 0 to 1 in increments of 0.1. The equations do not output probability values in such discrete intervals. Therefore, the probability values were organized into bins according to their rounded value. The number of 'yes' lightning observations in each bin were divided by the total number of forecast/observation pairs in each bin to get a reliability value for that bin. For example, if there were 10 pairs assigned to the 0.1 bin and one of the observations was 'yes' for lightning, the reliability would be [1 'yes' observation] / [10 forecast/observation pairs] or 0.1. The forecast is said to exhibit perfect reliability when the reliability is equal to the bin value.

The reliability diagrams for the P-1 and P-2 equations are shown in Figure 7. The black diagonal line represents perfect reliability. Where the curves are below the black line, the equations over-forecasted lightning occurrence, and where the curves are above the line, the equations under-forecast lightning occurrence. Both curves are mostly above the black line, indicating a tendency to under-forecast lightning occurrence. The red curve for the P-2 equations was closer to the perfect reliability diagonal than the blue curve for the P-1 equations for all probabilities except for 0.6 and 0.7. The number of samples used to calculate the reliability decreased with increasing forecast probability, which may account for the 20% over-forecast at 0.9 forecast probability. The increasing variability of the P-2 equations at higher probabilities is likely an artifact of the relatively small sample sizes at those larger probabilities and that variation is likely not statistically significant. Overall, these curves demonstrate that the P-2 equations have better reliability than the P-1 equations.

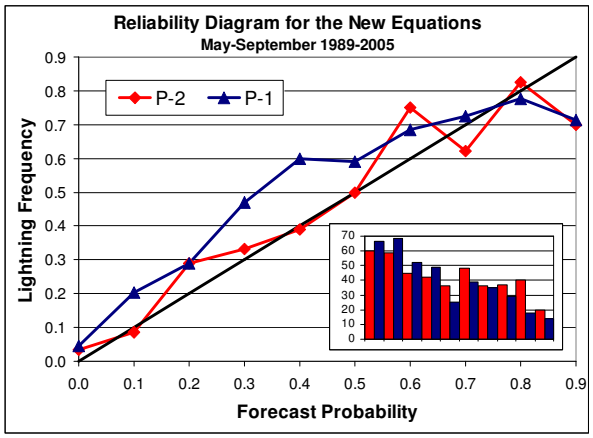

Figure 7. Reliability diagram of the P-1 and P-2 probability forecasts for all months. The black diagonal line represents perfect reliability, the blue curve represents the reliability of the P-1 equations, and the red curve represents the reliability of the P-2 equations. The histogram at the lower right shows the number of observations in each probability range for the old (blue) and new (red) forecast methods.

The extent of the under-forecasting was quantified by calculating the bias for each equation set. The forecasts and observation pairs for the entire warm season were used in the bias calculation. The average bias in percent was calculated using the equation

$$B = \frac{\sum_{i=1}^{i=N}(p_i - o_i)}{N} * 100,$$

where B is the bias in percent, o_i is the binary lightning observation, p_i is the associated probability forecast, and N is the number of observation/forecast pairs. The bias was -5.9% for the P-1 equations and -0.4% for the P-2 equations. The P-2 equations reduced the under-forecast bias by 4.5%.

Contingency Table Statistics

Forecast verification using a contingency table is most appropriate for categorical forecasts in which a phenomenon is forecast to occur or not. It is a less appropriate method for probability forecasts that express levels of uncertainty in which no probability value in the range 0–1 is necessarily wrong or right (Wilks 2006). Nonetheless, it is a familiar and easily understood method that can shed light on forecast performance provided an appropriate probability threshold value is defined, above which the forecast will be considered 'yes' and below which the forecast will be considered 'no'.

The proper threshold, or cutoff, value depends on the forecast decision issue to which the user will apply the forecast (Wilks 2006). The original goal of Phase I was to create equations that performed better than persistence, since persistence performed better than NPTI. The goal of Phase II was to improve the performance of the equations further. The AMU used the condition for the P-1 and P-2 equations that the threshold value chosen must outperform the persistence forecast for all of the contingency table values. The procedure used tested probability values from 0.1 to 0.9 in increments of 0.01. Details of the procedure are in Lambert (2007). The resulting threshold values were 0.35 for the P-1 equations and 0.47 for the P-2 equations. Table 5 contains the accuracy measures and skill scores for each set of equations using the cutoff values and those of their associated persistence forecasts. The P-2 equations exhibited better accuracy and skill than persistence and the P-1 equations.

Table 5. The accuracy measures and skill scores for the P-2 equations with a threshold cutoff probability of 0.47, the P-1 equations with a cutoff probability of 0.35, and the persistence (Pers) forecasts associated with each set of equations.

Statistic	***P-2 (0.47)***	***Pers (P-2)***	***P-1 (0.35)***	***Pers (P-1)***
POD	0.68	0.62	0.66	0.63
FAR	0.21	0.23	0.23	0.24
HR	0.74	0.71	0.73	0.71
CSI	0.52	0.46	0.50	0.47
HSS	0.47	0.40	0.44	0.40
KSS	0.47	0.39	0.44	0.40

Equation Performance Summary

The main goal for this task was to create new lightning probability forecast equations that would outperform the P-1 equations currently used in operations. The new P-2 equations did outperform the P-1 equations as evidenced by the four tests.

The SS values indicated that the equations showed an increase in skill over daily and monthly lightning climatology, persistence, and the flow regime lightning probabilities. For the entire warm season, the P-2 equations showed an 8% increase in skill over the P-1 equations. The P-1 equations showed a 48% improvement in skill over the NPTI in Phase I With the additional 8% gain in skill over the P-1 equations, the P-2 equations showed a total gain in skill of 56% over the NPTI. The P-1 equations were slightly better at distinguishing non-lightning days, but the P-2 equations were better at distinguishing lightning days (Figure 6). The P-2 equations demonstrated an improved reliability over the P-1 equations, and reduced the overall negative bias by almost 5% (Figure 7). Finally, the P-2 equations had the best accuracy measures and skill scores compared it their associated persistence forecasts and the P-1 equations (Table 5). Since most of the tests indicated that the P-2 equations exhibited superior performance over the P-1 equations, they replaced the P-1 equations before the start of the 2007 lightning season.

6. GRAPHICAL USER INTERFACE

In Phase I, the AMU created a GUI in Excel to facilitate user-friendly input to the equations and fast, easy-to-read output. The 45 WS was involved in the GUI development by providing comments and suggestions on the design to ensure the final product addressed their operational needs. With this GUI, the forecasters had to gather the predictor values from one system and enter them in the GUI on a separate computer. This step used time that could be spent doing other required duties, and increased the risk of entering an incorrect value resulting in an erroneous probability value. As part of Phase II, the AMU, assisted by Mr. Paul Wahner of Computer Sciences Raytheon (CSR), developed a similar GUI in MIDDS that gathers the required predictor values from the sounding automatically.

The MIDDS GUI was developed with the Tool Command Language (Tcl)/Toolkit (Tk) capability in MIDDS. The design and function of this GUI is similar to the Excel GUI, but goes one step further by loading the sounding predictor values automatically into the dialog box. This removes the risk of a forecaster entering an incorrect value while also reducing the time the forecaster would spend gathering and calculating the required parameter values. The GUI has two dialog boxes: the first displays the date and asks for equation predictor values, and the second displays the equation output.

Equation Predictor Dialog Box

The equation predictor dialog box(Figure 8) is displayed first. The dialog box has five tabs, one for each month. The tab of the current month is displayed initially. The current month, day and sounding time are printed along the top of the dialog box. If the current day's sounding is not available, "No Current Sounding" will be displayed in place of the date and time in the upper right. The day value can be changed by the up/down arrows or by entering a value manually in the text box. This allows forecasters flexibility when making the seven-day Weekly Planning Forecast. The sounding date and time is formatted by year, day of year, and UTC time.

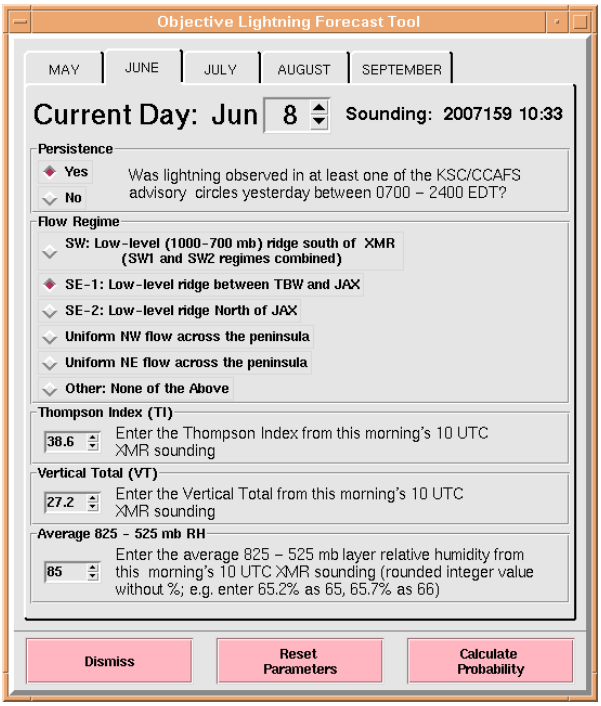

Figure 8. Equation predictor dialog box for June. A tab for each month is at the top, followed by the date and sounding time, then the predictor values. Clicking the "Dismiss" button closes the GUI, the "Reset Parameters" button resets the sounding stability parameters to original values, and the "Calculate Probability" button displays the probability output dialog box (Figure 9).

The user chooses Yes or No for persistence, and then a flow regime. They do not have to enter the sounding parameters since those values are already input by the GUI code and displayed in their associated text boxes. If there is not a current sounding, the text boxes will be populated with the values from the most recent sounding available. The "No Current Sounding" message in the top right corner will inform the forecaster that this is the case.

The final step is to click on the "Calculate Probability" button in the lower right corner of the dialog box. The "Dismiss" button in the lower left closes the GUI. If the forecaster does not choose a persistence value or flow regime, one of two error messages is displayed informing the forecaster that a choice needs to be made (not shown)

Output

When the user clicks the "Calculate Probability" button in the equation predictor dialog box, the probability of lightning occurrence for the day is displayed in a dialog box (Figure 9). The GUI code also outputs a file that contains all the parameter values input by the user to calculate the probability for later reference.

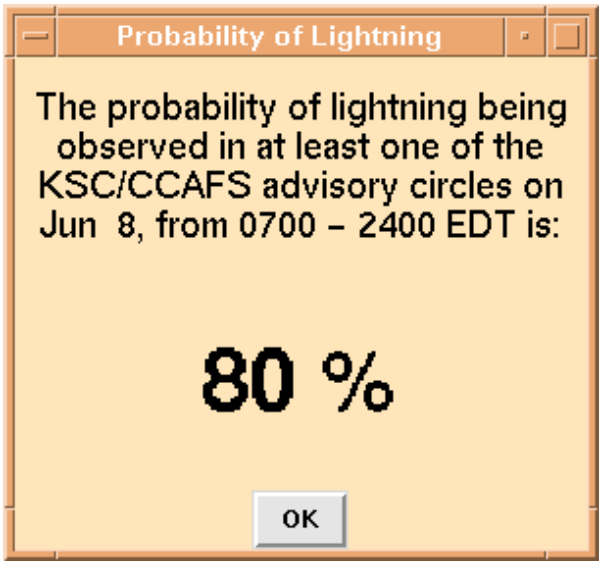

Figure 9. The dialog box displaying the probability of lightning occurrence for the day as calculated by the equation. Clicking the "OK" button closes the box.

7. FUTURE WORK

At the AMU Tasking Meeting in April 2007, a third phase to this task was approved in which two changes will be made in an effort to further improve equation performance. The first will be to include October data to the current POR. In looking at Figure 4a, it appears that the end of the lightning season is beyond September 30. The daily climatology values at the end of September are approximately 10% higher than at the beginning of May. The second modification will be to stratify the warm seasons by the progression of the daily climatology instead of by month. Stratifying the data by the progression of the daily climatology through the warm season is more meteorologically representative than by date. The AMU will develop a method to determine four to five sub-seasons in the overall warm season:

- A pre-lightning season in early May,
- A spin-up transition season from mid to late May to early or mid June,
- The core lightning season from early to mid June to mid or late August,
- A spin-down transition season through September, and
- A possible post-lightning season in October.

The number of sub-seasons cannot be determined until the October data are added and a new daily climatology chart is created. One equation will be developed for each sub-season and their performance compared to the P-2 equations.

Data from more years are planned to be added in future phases. This will help develop more robust statistical relationships in the equations and provide more data for verification. Also, new techniques may be available over the next few years that could help improve equation performance. Any such techniques should be considered and tested in future phases. Evaluation of equation performance should be done continuously to determine the tool's strengths and weaknesses, which can be used to guide future modifications.

8. SUMMARY AND CONCLUSIONS

The AMU created five logistic regression equations that predict the probability of cloud-to-ground lightning occurrence for the day in the KSC/CCAFS 5 n mi warning circles for each month in the warm season. These equations are based on equations developed in Phase 1 (Lambert and Wheeler 2005), but with five modifications:

- Increase the POR from 15 to 17 years (1989-2005),
- Modify the valid area to eliminate areas not within the 5 n mi warning circles,
- Include the XMR 1000 UTC sounding in determining the flow regime of the day,
- Use a different smoothing function for the daily lightning climatology, and
- Determine the optimal layer for the average RH calculation.

The P-2 equations described in this report outperformed the P-1 equations by an overall 8%, and showed better performance than the P-1 equations in four other tests. As a result, the new P-2 equations were added to the current set of tools used by the 45 WS to determine the probability of lightning for their daily planning forecast. The details of the Phase II work can be found in Lambert (2007).

Results from the P-2 equations are meant to be used as first-guess guidance when developing the lightning probability forecast for the day. They provide an objective base from which forecasters can use other observations, model data, consultation with other forecasters, and their own experience to create the final lightning probability for the 1100 UTC briefing.

9. REFERENCES

Bauman, W. H., W. P. Roeder, R. A. Lafosse, D. W. Sharp, and F. J. Merceret, 2004: The Applied Meteorology Unit – operational contributions to Spaceport Canaveral. Preprints, *11th Conference on Aviation, Range, and Aerospace Meteorology*, Amer. Meteor. Soc., Hyannis, MA, 24 pp.

Boyd, B. F., W. P. Roeder, D. Hajek, and M. B. Wilson, 2005: Installation, upgrade, and evaluation of a short baseline cloud-to-ground lightning surveillance system in support of space launch operations, *Conference on Meteorological Applications of Lightning Data*, Amer. Meteor. Soc., San Dieago, CA, 4 pp.

Everitt, J. A., 1999: An Improved Thunderstorm Forecast Index for Cape Canaveral, Florida. M.S. Thesis, AFIT/GM/ENP/99M-06, Department of Engineering Physics, Air Force Institute of Technology, 98 pp. [Available from the Air Force Institute of Technology, Wright-Patterson Air Force Base, OH 45433].

Harms, D. E., A. A. Guiffrida, B. F. Boyd, L. H. Gross, G. D. Strohm, R. M. Lucci, J. W. Weems, E. D. Priselac, K. Lammers, H. C. Herring and F.J. Merceret, 1999: The many lives of a meteorologist in support of space launch, *8th Conference On Aviation, Range, and Aerospace Meteorology*, Amer. Meteor. Soc., Dallas, TX, 5-9.

Howell, C. L., 1998: Nowcasting Thunderstorms At Cape Canaveral, Florida Using An Improved Neumann-Pfeffer Thunderstorm Index, M.S. Thesis, AFIT/GM/ENP/98M-05, Department of Engineering Physics, Air Force Institute of Technology, pp 93 [Available from the Air Force Institute of Technology, Wright-Patterson Air Force Base, OH 45433].

Insightful Corporation, 2005a: *S-PLUS 7 for Windows Guide to Statistics, Volume 1*, Insightful Corp., Seattle, WA, 730 pp.

Insightful Corporation, 2005b: *S-PLUS 7 for Windows User's Guide*, Insightful Corp., Seattle, WA, 664 pp.

Kelly, J. L., H. E. Fuelberg, and W. P. Roeder, 1998: Thunderstorm predictive signatures for the east coast sea breeze (ECSB) at Cape Canaveral Air Station (CCAS) and the Kennedy Space Center (KSC), *19th Conference on Severe Local Storms*, Amer. Meteor. Soc., Minneapolis, MN, 677-680

Lambert, W., 2007: Objective Lightning Probability Forecasting for Kennedy Space Center and Cape Canaveral Air Force Station, Phase II. . NASA Contractor Report CR-2007-214732, Kennedy Space Center, FL, 59 pp. [Available from ENSCO, Inc., 1980 N. Atlantic Ave., Suite 230, Cocoa Beach, FL, 32931, or http://science.ksc.nasa.gov/amu/final.html]

Lambert, W. and M. Wheeler, 2005: Objective Lightning Probability Forecasting for Kennedy Space Center and Cape Canaveral Air Force Station. NASA Contractor Report CR-2005-212564, Kennedy Space Center, FL, 54 pp. [Available from ENSCO, Inc., 1980 N. Atlantic Ave., Suite 230, Cocoa Beach, FL, 32931, or http://science.ksc.nasa.gov/amu/final.html]

Lazzara, M. A., J. M. Benson, R. J. Fox, D. J. Laitsch, J. P. Rueden, D. A. Santek, D. M. Wade, T. M. Whittaker, and J. T. Young, 1999: The Man computer Interactive Data Access System (McIDAS): 25 Years of Interactive Processing. *Bull. Amer. Meteor. Soc.*, **80**, 271 – 284.

Lericos, T., H. Fuelberg, A. Watson, and R. Holle, 2002: Warm season lightning distributions over the Florida Peninsula as related to synoptic patterns. *Wea. Forecasting*, **17**, 83 – 98.

Menard, S., 2000: Coefficients of determination for multiple logistic regression analysis. *American Statistician*, **54**, 17 – 24.

Neumann, C. J., 1971: Thunderstorm forecasting at Cape Kennedy, Florida, utilizing multiple regression techniques. NOAA Technical Memorandum NWS SOS-8.

Peppler, R. A. and P. J. Lamb, 1989: Tropospheric static stability and Central North American growing season rainfall. *Mon. Wea. Rev.*, **117**, 1156 – 1180.

Weems, J. W., C. S. Pinder, W. P. Roeder, and B. F. Boyd, 2001: Lightning watch and warning support to spacelift operations, *18th Conference on Weather Analysis and Forecasting*, Amer. Meteor. Soc., Ft. Lauderdale, FL, 301-305.

Wilks, D. S., 2006: *Statistical Methods in the Atmospheric Sciences*. 2d ed. Academic Press, Inc., San Diego, CA, 467 pp.

Roeder, W. P., and T. M. McNamara, 2006: A survey of the Lightning Launch Commit Criteria, *Second Conference on Meteorological Applications of Lightning Data*, Amer. Meteor. Soc., Atlanta, GA, 18 pp.

NOTICE